JOURNAL OF MATERIALS SCIENCE 31 (1996) 3281–3288

Mathematical and experimental investigation of the self-propagating high-temperature synthesis (SHS) of $TiAl_3$ and Ni_3Al intermetallic compounds

H. Y. SOHN, X. WANG,
Department of Metallurgical Engineering, University of Utah, Salt Lake City, UT 84112-1183 USA

One-dimensional mathematical modeling was used to describe the self-propagating high-temperature synthesis (SHS) process for preparing $TiAl_3$ and Ni_3Al intermetallics. The kinetic parameters (activation energies and pre-exponential factors) for the two compounds were obtained by matching experimental measurement and the numerical solution. The results thus obtained were compared with rate parameters obtained using different methods. The activation energy was 483 and 283 kJ mol^{-1} for the formation of $TiAl_3$ and Ni_3Al, respectively. The temperature profiles calculated using the mathematical model were compared with experimental measurements for both aluminides which indicated reasonable agreement. Fine particle size and moderate preheating increase the SHS rates.

Nomenclature

a	Thermal diffusivity, m^2 s^{-1}
c	Heat capacity, J K^{-1} mol^{-1}
E	Activation energy, J mol^{-1}
ΔH	Enthalpy, J mol^{-1}
I	$\int_0^1 \varphi \, dt + \int_0^1 (1-t)\varphi \, dt$, defined in Equation 29
k	Rate constant, s^{-1}
k_0	Pre-exponential factor, s^{-1}
m	Atomic fraction
n	Reaction order
p	Function defined by Equation 17
R	Gas constant, 8.314 J mol^{-1} K^{-1}
T	Temperature, K
t	Time, s
u	Burning rate, m s^{-1}
x	Distance, m

Greek Letters

α	Conversion fraction
λ	Thermal conductivity, W m^{-1} K^{-1}
ρ	Density, g cm^{-3}
σ	Constant in Equation 36
τ	Dimensionless temperature defined by Equation 12
φ	$\frac{(-\Delta H)\rho\phi}{T_{ad} - T_0}$ defined in Equation 13
Φ	function defined in Equation 2
ω	ρuc

Subscripts

0	Initial state or total
1	Substance 1
2	Substance 2
a	Substance a
avg	Average
ad	Adiabatic state
b	Substance b
f	Formation
ig	Ignition state
m	Mean
max	Maximum
s	Sample

1. Introduction

A substantial number of inorganic materials can be synthesized using their exothermic heats of formation by reacting mixtures of very fine powders of the constituent reactants [1–5]. In many cases, when one end of such a mixture is ignited, the reaction self-propagates through the rest of the mixture until all the reactants are consumed. The unique advantages associated with this process include the fact that a very high reaction temperature can be reached with a small amount of external energy. This group of reactions is of considerable interest in producing intermetallic compounds, ceramics, and composite materials. Among these materials, titanium and nickel aluminides have attracted a great deal of attention due to their high strength-to-weight ratio and high-temperature corrosion resistance [6–9]. The major shortcoming of these materials is their brittleness. Their ductility can, however, be improved by the addition of minor dopants as in the case of boron addition to Ni_3Al [10], Nb addition to TiAl and Ti_3Al [9] and Ti and Nb additions to NiAl [11].

The objective of this research was to study the SHS of the intermetallic compounds of nickel and titanium

0022–2461

aluminides, especially the Ni_3Al and $TiAl_3$ phases. A series of experiments was carried out to investigate the effects of various initial conditions on the SHS results. The products were examined using the electron microprobe (EPMA) energy-dispersed X-ray (EDAX), X-ray diffraction (XRD) and optical microscopy to determine the phases and their physical characteristics. The microhardness of the products was also measured to study the effects of initial variables. Most of the results on the effects of the experimental conditions on the properties of the product were summarized in an earlier paper [12]. In this article, the rates of the SHS of $TiAl_3$ and Ni_3Al intermetallic compounds are analysed. For this purpose, a unidirectional steady-state mathematical model was formulated. The kinetic parameters obtained by solving the model equation are compared with those obtained using an approximate solution available in the literature [2] and those obtained using differential scanning calorimetry (DSC) in this laboratory [13].

2. Mathematical modelling of unidirectional combustion

A unidirectional steady-state mathematical model for SHS based on heat transfer and chemical kinetics was formulated. The numerical solution to the model is described. The method for obtaining kinetic parameters from the observed burning rates and temperature profiles during SHS is given.

2.1. Model basis

One of the notable characteristics of the SHS process is the sharp temperature change with respect to time or space. In general, the sample is ignited at one end of the pellet, and the combustion front propagates through the pellet to the other end. It is reasonable to assume unidirectional reaction for the purpose of mathematical modeling.

The following assumptions are made in the development of the model [3]:

(I) The reaction proceeds in one direction.

(II) The sample is treated as a homogeneous continuum. The physical properties are isotropic.

(III) The effects of temperature on the thermal properties are small. Thus, averaged values of parameters are used.

(IV) The physical properties do not change significantly upon reaction, and the same property values can be used for the product(s) and the reactants.

(V) Heat loss to the surrounds is negligible.

2.2. Mathematical modeling

By performing an energy balance, the following governing equation based on the model assumptions is obtained [3, 14, 15]

$$\rho(-\Delta H)\Phi = -\frac{\partial}{\partial x}\left(\lambda\frac{\partial T}{\partial x}\right) + \rho c\frac{\partial T}{\partial t} \quad (1)$$

where Φ is the kinetics function given by

$$\Phi = \frac{d\alpha}{dt} = kf(\alpha) \quad (2)$$

and α is the fractional conversion and the rate constant k is given by the Arrhenius equation

$$k = k_0 \exp\left(-\frac{E}{RT}\right) \quad (3)$$

Combining Equations (1–3), the governing equation describing the unidirectional combustion can be written as

$$\frac{\partial}{\partial x}\left(\lambda\frac{\partial T}{\partial x}\right) - \rho c\frac{\partial T}{\partial t} + \rho(-\Delta H)k_0 f(\alpha)\exp\left(-\frac{E}{RT}\right) = 0 \quad (4)$$

with the following boundary conditions:

$$\text{for } t \leq 0,\ T = T_0,\ \alpha = 0 \quad (5)$$

$$\text{for } x = -\infty,\ T = T_0,\ \frac{\partial T}{\partial x} = 0,\quad \alpha = 0 \quad (6)$$

$$\text{for } x = \infty,\ T = T_{ad},\ \frac{\partial T}{\partial x} = 0,\ \alpha = 1 \quad (7)$$

After ignition, the SHS process can be treated as a steady-state problem with the burning front moving at a constant speed. For mathematical convenience, let the solid move in the direction of the distance coordinate at the same rate as the burning front. Then,

$$u = \frac{dx}{dt} \quad (8)$$

and

$$\frac{\partial T}{\partial t} = u\frac{\partial T}{\partial x} \quad (9)$$

Thus, the following steady-state model is formulated, assuming constant thermal conductivity:

$$\lambda\frac{d^2T}{d^2x} - \rho cu\frac{dT}{dx} + \rho(-\Delta H)k_0 f(\alpha)\exp\left(-\frac{E}{RT}\right) = 0 \quad (10)$$

The boundary conditions remain the same.

Since the rate function Φ involves fractional conversion α, it is necessary to relate it to other parameters. Integrating the governing Equation 4 between the limits $x = -\infty$ to any point x using boundary conditions for α, one obtains,

$$\alpha = \frac{\rho cu(T - T_0) - \lambda\frac{dT}{dx}}{\rho(-\Delta H)u} \quad (11)$$

Equation 10 with the boundary conditions forms the mathematical model for the unidirectional steady-state combustion for the SHS process. Solving these equations, the temperature profile can be calculated if the kinetic parameters, viz. activation energy, pre-exponential factor, and the form of the conversion factor, are known.

2.3. Solution of the model equations

There is no analytical solution to the governing equations. Direct numerical solution of the equations is difficult since it involves a stiff problem, which is caused by the steep temperature increase with distance [16,17]. Because the chemical reaction is highly exothermic, a simplified solution may be used [18–21]. It is convenient to define the following dimensionless variables:

$$\tau = \frac{T - T_0}{T_{ad} - T_0} \tag{12}$$

$$\varphi(\tau) = \frac{(-\Delta H)\rho\Phi(T)}{T_{ad} - T_0} \tag{13}$$

Equation 10 and the boundary conditions are rewritten in terms of τ:

$$\lambda\frac{d^2\tau}{dx^2} - \rho uc\frac{d\tau}{dx} + \varphi(\tau) = 0 \tag{14}$$

$$x = -\infty,\ \tau = 0,\ \frac{d\tau}{dx} = 0 \tag{15}$$

$$x = +\infty,\ \tau = 1,\ \frac{d\tau}{dx} = 0 \tag{16}$$

Since x does not appear explicitly in the equation, let

$$p = \lambda\frac{d\tau}{dx} \tag{17}$$

When the following term is introduced,

$$\omega = \rho uc \tag{18}$$

the governing equation becomes

$$p\frac{dp}{d\tau} - \omega p + \varphi(\tau) = 0 \tag{19}$$

with boundary conditions

$$\tau = 0,\quad p = 0 \tag{20}$$

$$\tau = 1,\quad p = 0 \tag{21}$$

Rewriting Equation 11,

$$\alpha = \frac{\omega\tau - \lambda p}{\rho(-\Delta H)u} \tag{22}$$

The governing equation can be further simplified by considering that Φ is a very strong function of temperature [19]. At low temperatures, the chemical reaction is weak, and therefore Equation 19 becomes

$$p\frac{dp}{d\tau} - \omega p = 0 \quad (\tau \le \tau_{ig}) \tag{23}$$

Applying boundary condition 20 to Equation 23, we get

$$p = \omega\tau \quad (\tau \le \tau_{ig}) \tag{24}$$

At high temperatures, the chemical reaction is very fast, and the term involving the sensible heat is negligible. Therefore, Equation 19 becomes

$$p\frac{dp}{d\tau} + \varphi(\tau) = 0 \tag{25}$$

Applying the boundary condition 21 to solve Equation 25, we get

$$p(\tau) = \left(2\int_\tau^1 \varphi(\tau)\,d\tau\right)^{1/2} \quad (\tau \ge \tau_{ig}) \tag{26}$$

The solution to Equation 19 is a combination of Equations 24 and 26. The existence and uniqueness of the solution to Equation 14 have been proved [19, 20].

Since the solution to Equation 19 should be continuous, at the ignition temperature we have

$$\omega\tau_{ig} = \left(2\int_{\tau_{ig}}^1 \varphi(\tau)\,d\tau\right)^{1/2} \quad (\tau = \tau_{ig}) \tag{27}$$

where τ_{ig} is the value of τ at which Equations 24 and 26 intersect.

For a given temperature profile and kinetics and physical property parameters, the burning rate u is determined by Equation 27, since $\omega = \rho uc$. However, this equation overestimates u. Zeldovich [19,20] obtained the range for u as follows:

$$\frac{I}{\rho c} < u < \frac{2^{1/2}I}{\rho c} \tag{28}$$

where I is defined as follows:

$$I = \int_0^1 \varphi(t)\,dt + \int_0^1 (1-t)\varphi(t)\,dt \tag{29}$$

2.4. Obtaining kinetic parameters from combustion theory

From the combustion theory, as discussed previously, the burning rate is determined based on the kinetic parameters such as E, k_0, and temperature profile. However, it is more often necessary to obtain the kinetic parameters from the temperature profile and the measured burning rate by applying the theory. Kanuary [22] classified this problem as an inverse problem to the combustion theory.

The mathematical desription of the inverse problem is defined by Equations (4–7). The unknown parameters are the activation energy E and pre-exponential factor k_0, as well as the function $f(\alpha)$. Parameters such as ρ, λ, c_p, and $(-\Delta H)$ can be obtained from the literature or measurement. The solution to the inverse problem requires the determination of E and k_0 by solving the differential equations based on those known parameters and experimental results.

It is clear that the solution for Φ cannot be obtained from Equations 24 and 26 directly. A proper approach to the solution is a trial-and-error method, comparing the calculated results with the measured results until the comparison is satisfied.

It is necessary to know the form of $f(\alpha)$ when obtaining E and k_0. Because of the dominant effect of $\exp(-E/RT)$, the form of $f(\alpha)$ does not affect the function of Φ strongly. The form of $f(\alpha)$ was determined in this work by a DSC study to be $(1-\alpha)^2$ [13,23].

To obtain the kinetic parameters E and k_0, a trial-and-error method with numerical iteration is necessary. Since the reaction rate is very low below the

ignition temperature, it is reasonable to assume Φ is 0 when $\tau < \tau_{ig}$. Then, the following approximation can be established:

$$\int_0^1 \varphi \, d\tau = \int_0^{\tau_{ig}} \varphi \, d\tau + \int_{\tau_{ig}}^1 \varphi \, d\tau \approx \int_{\tau_{ig}}^1 \varphi \, d\tau \quad (30)$$

From Equation 27,

$$\int_{\tau_{ig}}^1 \varphi \, d\tau = \frac{(\omega\tau_{ig})^2}{2} \quad (31)$$

Thus,

$$\int_{\tau}^1 \varphi \, d\tau = \int_{\tau_{ig}}^1 \varphi \, d\tau - \int_{\tau_{ig}}^{\tau} \varphi \, d\tau = \frac{(\omega\tau_{ig})^2}{2} - \int_{\tau_{ig}}^{\tau} \varphi \, d\tau \quad (32)$$

With repeated trial-and-error iterations, a right temperature profile that corresponds to the experimental results of the burning rate and the temperature-spatial coordinate can be found. Further details of the solution procedure can be found elsewhere [23].

3. Experimental methods

Elemental powders of Al, Ti, and Ni were used in the experiments. The Al powder was from Alfa Morton Thiokol, Ti from Micron Metals, and Ni from EM Science. The purity of the powders was 99% wt %. Different sizes of Ti and Ni particles were obtained by screening the powders under an argon atmosphere. Appropriate amounts of the pure powders for Ti + 3Al and 3Ni + Al mixtures were weighed and mixed in a roller for over three hours. The mixtures were then pelletized in a double-action press to form a rectangular pellet. The average size of the pellet was about 6 cm in length and 1.5 cm^2 in cross-section. The pellets were usually 60% of the full density. Several small holes were drilled into the pellets about one fourth of the pellet thickness to accommodate thermocouples.

Ignition was accomplished by a silicon carbide heating element, which was placed about 1–2 mm above the sample pellet. All sides of the pellets were covered by an insulating material except the top for ignition and the front side for observation of the burning rate. The sample was heated as quickly as possible to the ignition temperature. Thermocouples were connected to a data acquisition unit for recording the temperature–time data. A camcorder was used to record the burning rate. The process was conducted under an argon atmosphere. When the temperature of the sample reached the ignition temperature, a very bright layer was observed, which advanced from the top of the pellet to the bottom. Power to the heating element was disconnected immediately after the reaction started.

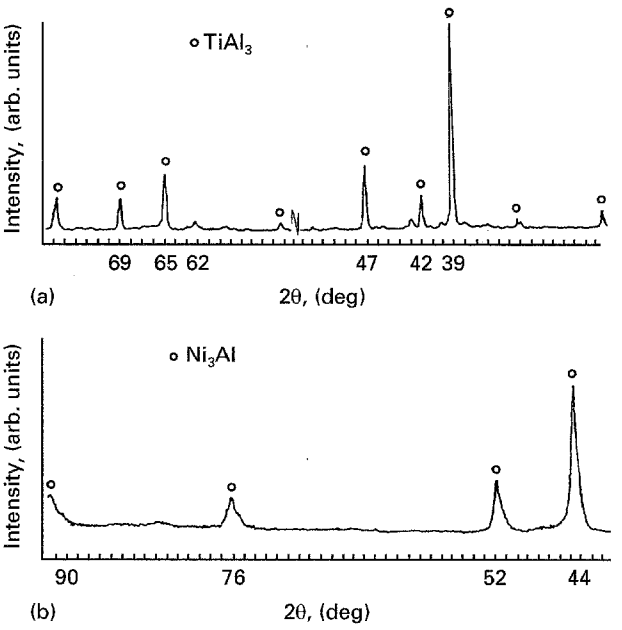

Figure 1 X-ray diffraction patterns of SHS products. (a) Ti + 3Al (b) 3Ni + Al.

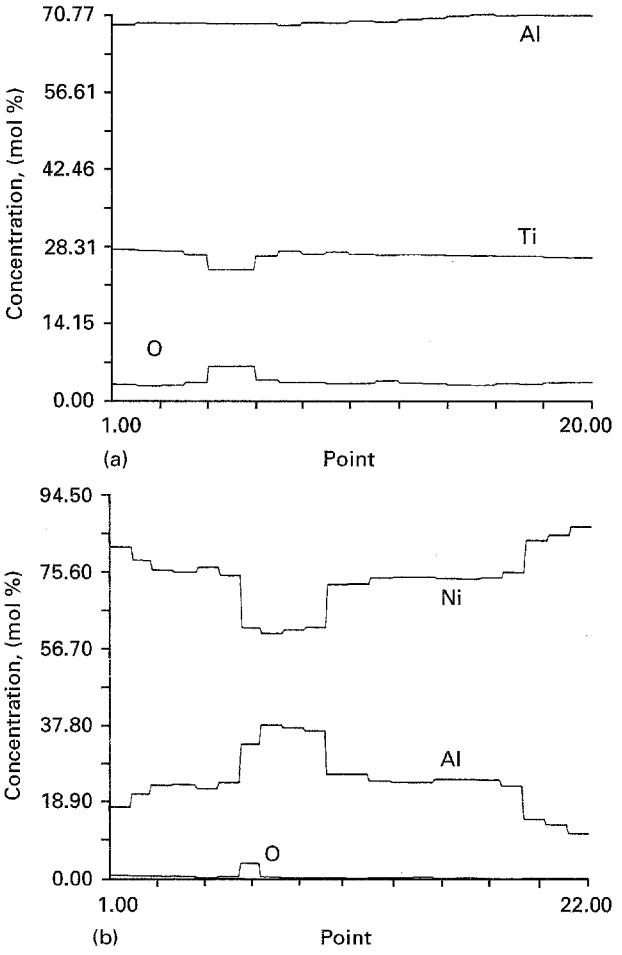

Figure 2 Electron microprobe analysis of product. (a) Ti + 3Al (b) 3Ni + Al.

4. Results of experiments

The composition of the products from the mixtures of Ti + 3Al and 3Ni + Al were analysed by XRD, and a typical diffraction pattern is shown in Fig. 1. The peaks indicate that the products are, respectively, $TiAl_3$ and Ni_3Al. An electron microprobe was used as an additional tool to examine the composition. Fig. 2 shows the composition profile of a point (~ 20 μm) for each product. The profiles show relatively constant compositions. It is therefore concluded that the SHS

products of $TiAl_3$ and Ni_3Al are basically single-phase products.

The density of the $TiAl_3$ product was about 70–80% of the full density, and that of Ni_3Al was about 90% of the full density. The overall shape of the products remained relatively unchanged from that of the green pellet except for some swelling for $TiAl_3$ and shrinking for Ni_3Al.

The temperature–time curves at several thermocouple locations within the pellets containing Ti + 3Al and 3Ni + Al are shown in Fig. 3 (a, b). It is seen that the curves for 3Ni + Al have much sharper slopes (Fig. 3b) than those for Ti + 3Al (Fig. 3). This is because the former system has a much greater burning rate than the latter, as can be seen from the time scale. The respective burning rates will be discussed in more detail later.

The thermocouple near the top of the pellet for 3Ni + Al (No. 1 in Fig. 3b) indicates that, at this point, the temperature rises slowly during the application of the ignition heating until it reaches the ignition temperature which in this case is 710 °C. Other curves taken at the middle and lower parts of the pellet show little heating until the reaction front reached these points. It can be seen that at these positions the temperature–time curves are the same, indicating that a steady combustion stage has been established. For stable planar combustion, as in these cases, the temperature–distance curves at steady-state can be obtained from the temperature–time curves with the aid of the measured burning rate.

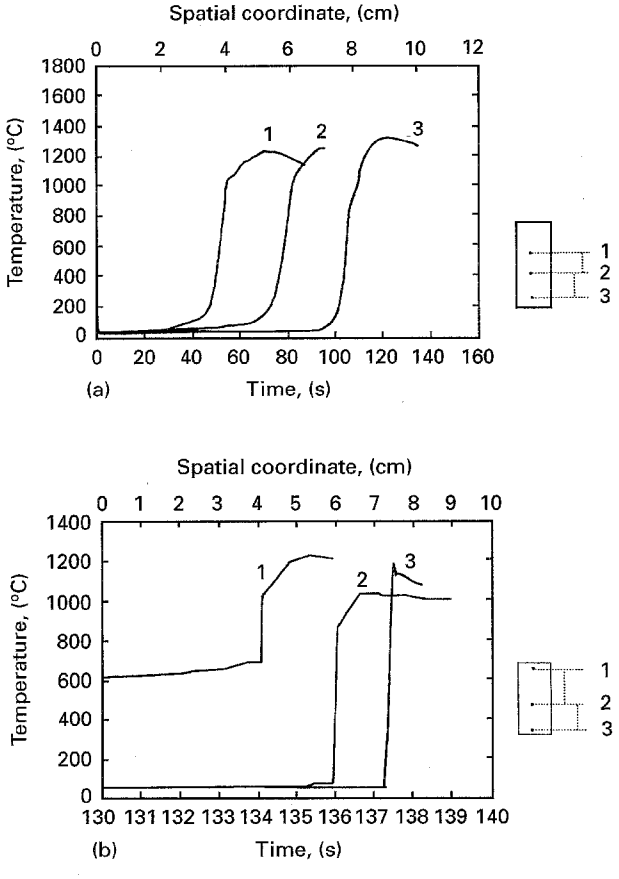

Figure 3 SHS temperature profiles. (a) Ti + 3Al (b) 3Ni + Al.

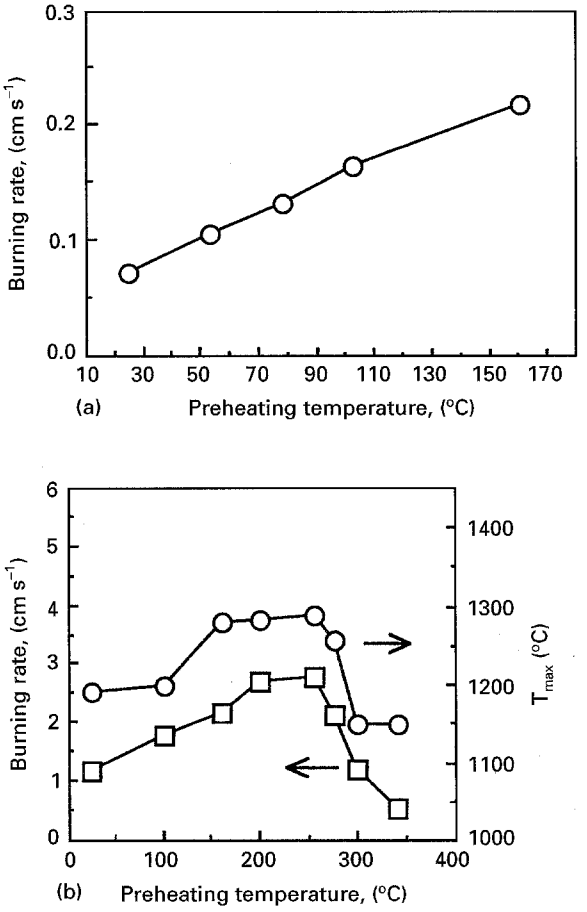

Figure 4 Effect of preheating on burning rate. (a) Ti + 3Al (b) 3Ni + Al (also maximum reaction temperature).

The effect of preheating the reactant pellet prior to ignition on the burning rate was examined. Heating experiments were conducted using a furnace around the pellet. The pellet was heated at a rate of about 100 °C per min to a desired temperature and then held for 5 min. The nominal particle sizes for Al, Ti, and Ni were −45, −45, and −10 μm, respectively. Fig. 4(a, b) illustrates the effect of preheating on the formation of $TiAl_3$ and Ni_3Al, respectively. Preheating to a moderate temperature increases the burning rate, as expected. However, excessive preheating was detrimental to the burning rate, as can be seen in Fig. 4b. This is because some reaction takes place at the contact points between the two solids, which inhibits the direct contact of molten aluminium with the other reactant after ignition. Furthermore, the heat produced by the premature reaction during preheating is largely lost to the surroundings and does not contribute to the SHS process after ignition.

5. Comparison between SHS experimental results and model predictions

As discussed in the mathematical modeling section, kinetic parameters such as activation energy and pre-exponential factor were obtained by solving the governing equation and comparing the solution to the experimental results. In this part, a detailed procedure

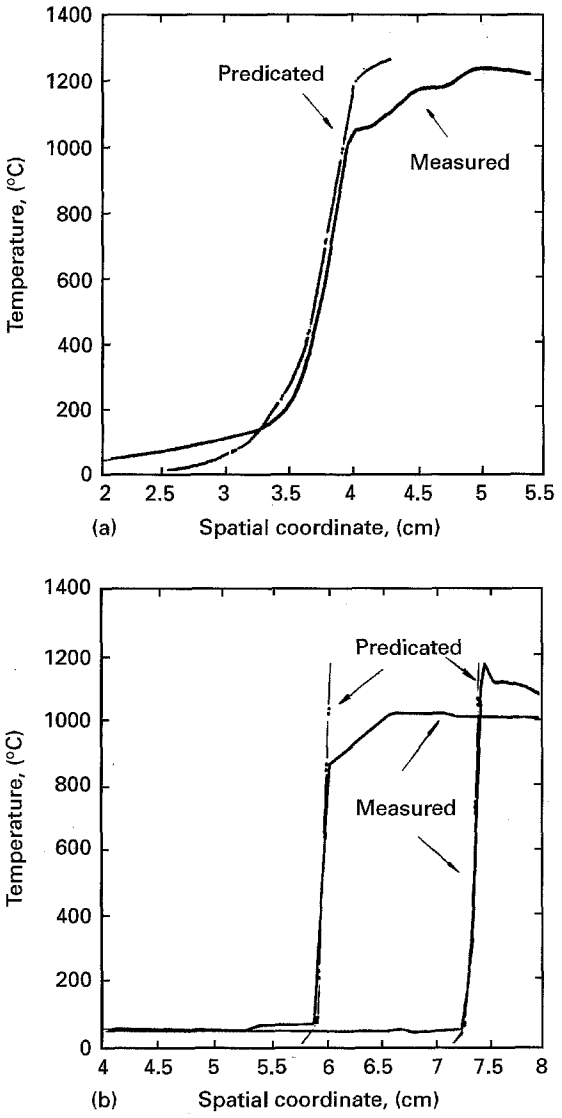

Figure 5 Mathematical model prediction of temperature profile. (a) Ti + 3Al (b) 3Ni + Al.

of the solution is illustrated. Selection methods for thermal conductivity, heat capacity, and reaction heat are discussed, and the kinetics of $TiAl_3$ and Ni_3Al are presented.

The adiabatic temperature T_{ad} is one of the boundary conditions needed in Equation 7 and was estimated based on thermodynamics. Assuming the sample to be a homogeneous continuum with constant physical properties, the adiabatic temperature can be evaluated by

$$(-\Delta H^0_{fT_0}) = \int_{T_0}^{T_{ad}} C_{P_s}\,dT \qquad (33)$$

where T_{ad} is adiabatic temperature, T_0 is the initial temperature, $(-\Delta H^0_{fT_0})$ is the enthalpy of reaction at temperature T_0, and C_{ps} is the heat capacity of the product. The values of T_{ad} are given in Table I.

The heat capacity C_p and density ρ were obtained from the literature [24, 25]. These parameters vary with temperature, and in order to select the representative values, their average values were calculated by

$$Y_{avg} = \frac{\int_{T_1}^{T_2} Y\,dt}{T_2 - T_1} \qquad (34)$$

TABLE I Results of the parameter selections

	$Ti_{0.25}Al_{0.75}$	$Ni_{0.75}Al_{0.25}$
$\lambda(W\cdot K^{-1}cm^{-1})$	3.1×10^{-2}	1.6×10^{-2}
$c(J\cdot mol^{-1}\cdot K^{-1})$	29.4	32.4
$(-\Delta H)(kJ\,mol^{-1})$	37.0 [30, 31]	40.3 [32]
$\rho(g\,cm^{-3})$	1.6	4.7
$T_0(K)$	298	298
$T_{ad}(K)$	1556 (1283 °C)	1542 (1269 °C)

It is difficult to obtain the physical properties of the product intermetallic compounds due to the lack of information. In this study, the differences between the reactant and product properties were neglected. The thermal conductivities of solid aluminium, titanium, and nickel as functions of temperature are known. However, the thermal conductivity of a porous pellet is difficult to estimate [26–28].

Experimental measurements on the thermal conductivities of metal powder compacts showed that they range mostly between 1–3% of the thermal conductivity of the solid phase [28]. For the pellets used in this work, a similar ratio is expected. In order to reduce the degree of uncertainty, however, the thermal conductivities of the sample pellets were obtained by matching Equation 24 with the portion of the measured temperature profile below the ignition temperature. These values are listed in Table I. They are indeed within 1–3% of the calculated average thermal conductivities of solid phases obtained from the literature [29].

The average heat capacity of the pellet from 298 K to the adiabatic temperature was computed for the mixture A_aB_b by the following equation:

$$c = m_a c_a + m_b c_b \qquad (35)$$

where c is the atomic heat capacity, m is the atomic fraction, and a and b denote the stoichiometry coefficients. Table I presents the results together with the average density values similarly obtained.

5.1. SHS kinetics of $TiAl_3$ and Ni_3Al formation

The kinetics of formation of the intermetallic compounds $TiAl_3$ and Ni_3Al were obtained by using the numerical solution of the model [Equation 14] compared with the results of the SHS experiments. Fig. 5(a, b) show the results of mathematical simulation and experiments for particles sizes −10 μm of Ni and −45 μm of Al and Ti. The activation energies of $TiAl_3$ and Ni_3Al formation are 483 kJ mol^{-1} and 265 kJ mol^{-1}, respectively. A pre-exponential factor of $6.2\times10^{17}\,s^{-1}$ was estimated for $TiAl_3$ and $1.6\times10^{11}\,s^{-1}$ for Ni_3Al.

5.2. Comparison

The following approximate solution for the burning rate as a function of the kinetic and thermodynamic parameters has been reported in the literature [22]. This solution was obtained by assuming that the

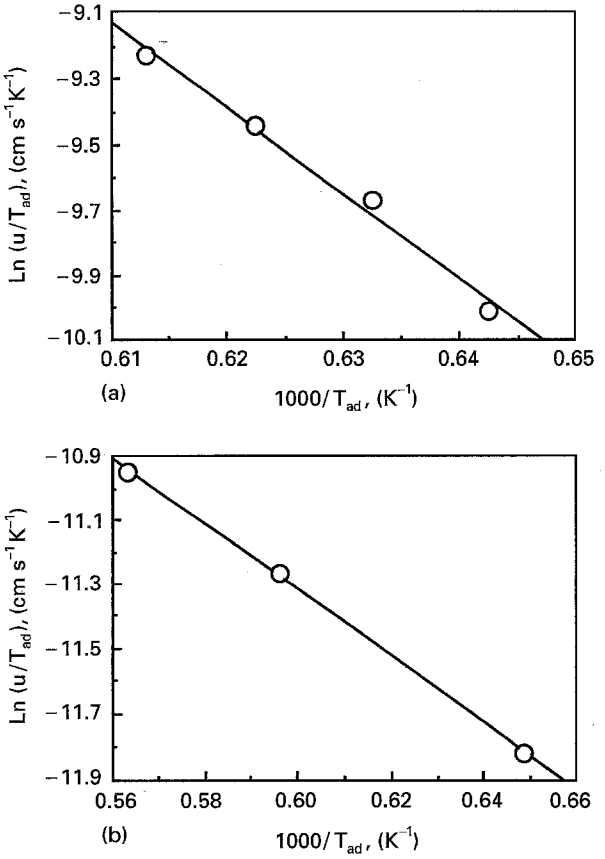

Figure 6 Plot of burning rate to calculate rate parameters according to Equation 36 (u in cm s^{-1}; T_{ad} in K). (a) Ti + 3Al (b) 3Ni + Al.

TABLE II Kinetics parameters from different methods

	Model	DSC	Equation (36)
$TiAl_3$ E(kJ mol^{-1})	483	517	439
k_0(s^{-1})	6.2×10^{17}	1.9×10^{23}	5.1×10^{19}
Ni_3Al E(kJ mol^{-1})	265	–	176
k_0(s^{-1})	1.6×10^{17}	–	2.8×10^{9}

reactants are completely converted in a region near the maximum combustion temperature:

$$u^2 = \sigma a \frac{c}{(-\Delta H)} \frac{RT_{ad}^2}{E} k_0 \exp\left(-\frac{E}{RT_{ad}}\right) \quad (36)$$

where for a first-order reaction, $\sigma = 1.1$; for a second-order reaction, $\sigma = 0.73$; and a is the thermal diffusivity.

According to Equation 36, the E and k_0 can be obtained from the values of the burning rate at different initial temperatures, by plotting Ln (u/T_{ad}) against $1/T_{ad}$, as shown in Fig. 6(a, b). The kinetics of $TiAl_3$ formation were also measured by using differential scanning calorimetry (DSC) [13]. The kinetic parameters from the SHS model, Equation 36, and DSC are listed in Table II. To compare the kinetics results, the results of E and k_0 from different methods were combined into the Arrhenius equation: $k = k_0 \exp(-E/RT)$, and the values of k at different temperature were calculated and compared, as shown in Fig. 7 (a, b). For $TiAl_3$, the rate constants by the DSC and

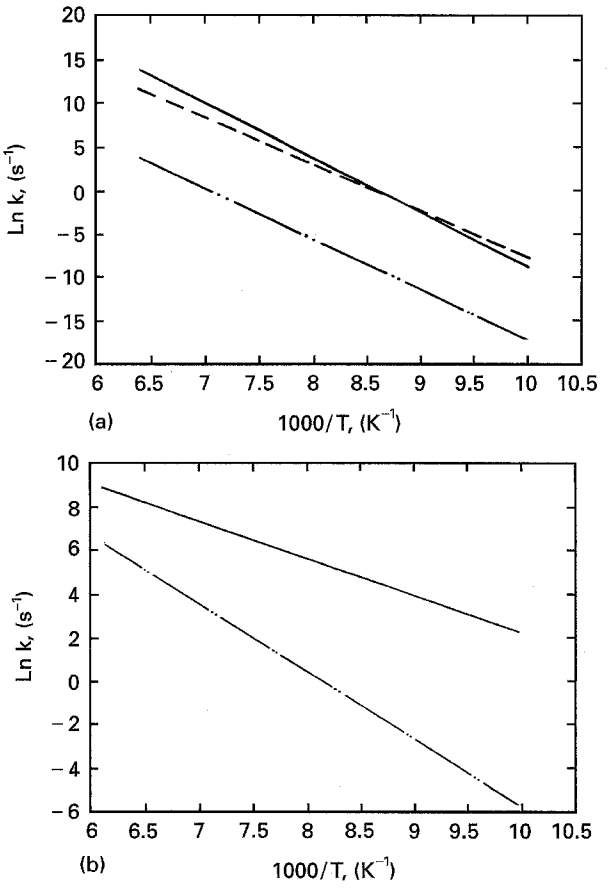

Figure 7 Comparison of rate constants obtained using different methods (—— DSC, – – – Equation 36, –·–· SHS modelling). (a) Ti + 3Al (b) 3Ni + Al.

Equation 36 are close, but both methods give values that are somewhat higher than that from the SHS model. For Ni_3Al, the rate constant obtained from Equation 36 is also higher than that from the SHS model.

6. Conclusions

An experimental investigation on the preparation of Ni_3Al and $TiAl_3$ by the SHS process has been conducted. A unidirectional steady-state mathematical model based on heat transfer and chemical kinetics was used to simulate the SHS process. Theoretical SHS temperature profiles calculated from the numerical solution of the model were close to the experimental data. By solving the model equation, the activation energy and the pre-exponential factor for the reaction were computed based on the observed burning rate and temperature profile. The kinetic parameters obtained from the DSC work and the SHS modeling agreed quite well. The model can be used to simulate the SHS process and obtain kinetics information for a unidirectional SHS reaction.

Acknowledgements

This work was supported in part by the Department of the Interior's Mineral Institutes program administered by the Bureau of Mines under allotment grant

Nos. G1184149, G1194149, and G1104149, the State of Utah Mineral Leasing Fund, and the University of Utah Research Committee Grant.

References

1. Z. MUNIR, *Ceram. Bull.* **67** (1988) 342.
2. A. G. MERZHANOV and I. P. BOROVINSKAYA, *Combustion Science and Technology* **10** (1975) 195.
3. W. I. FRANKHOUSER, K. W. BRENDLEY, M. C. KIESZEK, and S. T. SULLIVAN, *Gasless Combustion Synthesis of Refractory Compounds*, Noyes Publications, Park Ridge, New Jersey (1985) pp 5–60, 106–117.
4. V. HLAVACEK, *Ceram. Bull.* **70** (1991) 240.
5. A. G. MERZHANOV and I. P. BOROVINSKAYA, *Doklady of the Academy of Sciences of the U.S.S.R. Earth Sciences Sections* **204** (1972) 366.
6. A. I. TAUB and R. L. FLEISCHER, *Science* **243** (1989) 616.
7. V. K. SIKKA, Symposium Proceedings, *High Temperature Aluminides and Intermetallics*, October 1–5, 1989, Indianapolis, Indiana, edited by S. H. Whang, C. T. Liu, D. P. Pope, and J. D. Stiegler, The Minerals, Metals and Materials Society, Warrendale, Pennsylvania (1990) pp. 505–519.
8. D. E. ALMAN and N. S. STOLOFF, *Int. J. Powd. Met.* **27** (1991) 29.
9. J. M. LARSEN, K. A. WILLIAMS, S. J. BALSONE, and M. A. STUCK, Symposium Proceedings, *High Temperature Aluminides and Intermetallics*, October 1–5, 1989, Indianapolis, Indiana, edited by S. H. Whang, C. T. Liu, D. P. Pope, and J. D. Stiegler, The Minerals, Metals and Materials Society, Warrendale, Pennsylvania (1990) pp. 521–536.
10. C. T. LIU, C. L. WHITE and J. A. HORTON, *Acta Metall.* **33** (1985) 213.
11. W. A. KAYSSER, R. LANG, J. C. MURRAY and G. E. PETZOW, *Int. J. Powd. Metall.* **27** (1991) 43.
12. H. Y. SOHN and X. WANG, *Materials and Manufacturing Processes* **9** (1994) 75.
13. X. WANG, H. Y. SOHN and M. E. SCHLESINGER, *Materials Sci. Eng. A*, **A186** (1994) 151
14. G. E. MYERS, *Analytical Methods in Conduction Heat Transfer*, 2nd edn., McGraw-Hill, New York (1987) pp. 100–130.
15. R. B. BIRD, W. E. STEWART, and E. N. LIGHTFOOT, *Transport Phenomena*, Wiley, New York (1960) pp. 265–341.
16. A. A. ZENIN, A. G. MERZHANOV and G. A. NERSISYAN, *Physics of Combustion and Explosions* **17** (1981) 79.
17. M. G. ROTH, Ph.D. thesis, Department of Computer Science, University of Illinois at Urbana-Champaign (1984).
18. A. G. MERZHANOV, *Combustion and Flame* **16** (1971) 89.
19. Y. B. ZELDOVICH, G. I. BARENBLATT, V. B. LIBROVICH, and G. M. MAKHVILADZE, The *Mathematical Theory of Combustion and Explosions*, 1st ed., Consultant Bureau, A Division of Plenum Publishing Corporation, New York (1985) pp. 100–120, 305–341.
20. Y. A. ZELDOVICH: *J. Phys. Chem.* (*Zh. Fiz. Khim*) **4** (1930) 22.
21. A. G. MERZHANOV, *Combustion and Flame* **13** (1969) 143.
22. A. M. KANUARY, Introduction to Combustion Phenomena, Gordon and Breach Science Publishers, New York, (1975) pp. 297–299.
23. X. WANG, Ph.D. Dissertation, University of Utah, Salt Lake City, Utah (1993).
24. R. HULTGREN, *Selected Values of the Thermodynamic Properties of the Binary Alloys*, American Society for Metals, Metals Park, Ohio (1973) pp. 98–200.
25. R. A. ROBIC, B. S. HEMINGWAY, and J. R. FISHER, *U.S. Geological Survey Bulletin 1452*, United States Government Printing Office, Washington, DC, 1978, pp. 2–85.
26. J. SZEKELY, J. W. EVANS and H. Y. SOHN, *Gas-Solid Reactions*, Academic Press, New York (1976) pp. 206–246.
27. H. W. GODBEE and W. T. ZIEGLER, *J. Appl. Phys.* **37** (1966) 40–55, 56–61.
28. A. V. LUIKOV, A. G. SHASHKOV, O. L. VASILIEV and Y. E. FRAIMAN, *Int. J. Heat Mass Transfer* **11** (1966) 117.
29. C. Y. HO, R. W. POWELL and P. E. LILEY, *J. Phys. Chem. Ref. Data* **1** (1972) 279.
30. J. M. SYUVE and M. J. FERRANTE, "Low-Temperature Heat Capacity and High Temperature Enthalpy of $TiAl_3$", *Report of Investigation 7834, United States Department of Interior, Bureau of Mines* (1974) pp. 1–9.
31. W. W. LIANG, *Computer Coupling of Phase Diagrams and Thermochemistry*, **7** (1983) 13.
32. V. I. BOGDANOV, A. V. RUBAN and D. L. FUKS, *Russ. J. Phys.* **60** (1986) 1013.

Received 10 November 1994
and accepted 20 November 1995